Climate Dynamics (1997) 13 : 883–904

Climate
Dynamics

Patterns of low-frequency variability in a three-level quasi-geostrophic model

S. Corti,[1,2,*] **A. Giannini,**[1,3] **S. Tibaldi,**[1] **F. Molteni**[2]

[1]Atmospheric Dynamics Group, Department of Physics, University of Bologna, Italy
[2]CINECA, Casalecchio di Reno, Bologna, Italy
[3]Lamont-Doherty Earth Observatory, Palisades, NY 10964, USA

Received: 30 January 1997 / Accepted: 17 June 1997

Abstract. To assess the extent to which atmospheric low-frequency variability can be ascribed to internal dynamical causes, two extended runs (1200 winter seasons) of a three level quasi-geostrophic model have been carried out. In the first experiment the model was forced by an average forcing field computed from nine winter seasons; in the second experiment we used a periodically variable forcing in order to simulate a seasonal cycle. The analysis has been focused on the leading Northern Hemisphere teleconnection patterns, namely the Pacific North American (PNA) and the North Atlantic Oscillation (NAO) patterns, and on blocking, both in the Euro-Atlantic and Pacific sectors. The NAO and PNA patterns are realistically simulated by the model; the main difference with observations is a westward shift of the centres of action of the NAO. Related to this, the region of maximum frequency of Atlantic blocking is shifted from the eastern boundary of the North Atlantic to its central part. Apart from this shift, the statistics of blocking frequency and duration compare favourably with their observed counterparts. In particular, the model exhibits a level of interannual and interdecadal variability in blocking frequency which is (at least) as large as the observed one, despite the absence of any variability in the atmospheric energy sources and boundary conditions on such time scales.

1 Introduction

The question of the relative roles of internal atmospheric dynamics and variations in boundary forcing from the Earth's surface in the generation of extratropical low-frequency variability has long been debated in the meteorological community. The fact that the extratropical teleconnection patterns identified by Wallace and Gutzler (1981) resemble both atmospheric anomalies associated with strong ENSO events (e.g. Horel and Wallace 1981) and Rossby stationary waves excited by tropical diabatic heating (e.g. Hoskins and Karoly 1981) suggested a tropical origin for these large-scale anomalies, with tropical ocean temperature being the ultimate source of anomalous forcing. On the other hand, a number of long integrations of general circulation models performed with climatological sea-surface temperatures (SSTs) proved that extratropical low-frequency variability with realistic amplitude and spatial patterns could be generated even in the absence of anomalies in boundary conditions (e.g. Lau 1981; Branstator 1985a, b, 1990). In order to reconcile these (apparently) contradictory facts, it has been proposed that the effect of anomalous boundary forcing may be to alter the stability (and therefore the residence time) of extratropical 'regimes' which are generated by internal extratropical dynamics, in such a way that one particular regime becomes much more persistent in the presence of a given diabatic forcing anomaly (Molteni et al. 1993; Palmer 1993).

It has been demonstrated that tropical interannual variability would be much reduced in the absence of variations in ocean temperatures (e.g. Palmer 1987). The forcing mechanism advocated by Hoskins and Karoly (1981), however, is not necessarily restricted to diabatic heating anomalies induced by SSTs. Intraseasonal tropical variability such as that associated with the Madden-Julian Oscillation (Madden and Julian 1971) may substantially modify the distribution of tropical diabatic heating, and consequently have a feedback onto the mid-latitude flow. Therefore, one cannot rule out a role of tropical diabatic heating in determining the statistical properties of extratropical variability, even in the presence of time-constant SSTs.

A way to investigate this problem is to simulate extratropical variability with a relatively simple model in which the 'sources' of heat and momentum are fixed to seasonally averaged fields. In terms of quasi-geostrophic (QG) dynamics, this is equivalent to fixing the sources of QG potential vorticity. With this approach, atmospheric

Correspondence to: S. Corti

Present address:
*c/o CINECA, Via Magnanelli 6/3, Casalecchio di Reno, I-40033 Bologna, Italy

variability only arises because of the chaotic nature of the extratropical circulation, whereas the role of the tropical flow is simply to provide realistic lateral boundary conditions for the propagation of waves generated in midlatitudes.

The importance of the Earth's spherical geometry in determining the spatial pattern of the observed large-scale anomalies has been stressed in many studies. In the 'standard' QG approximation (e.g. Holton 1992), it is not possible to define a model which is both energetically consistent and properly tuned for both tropical and extratropical dynamics (see Mak 1991 for a detailed analysis). However, hemispheric QG models have been used by a number of investigators (e.g. Roads 1987; Marshall and So 1990) in order to simulate atmospheric low-frequency variability in a realistic geometric framework. Marshall and Molteni (1993, MM93 hereafter) showed that, when a QG model is formulated in terms of prognostic equations for QG potential vorticity, the same equations are valid for both the Northern and the Southern Hemisphere, and a global model can be defined which avoids potential problems of spurious wave reflection at the Equator. In MM93, such a model has been shown to produce a very realistic simulation of extratropical variability and flow regimes.

The specification of the potential vorticity sources is crucial in determining both the mean flow and the variability of a QG model. In MM93, these sources were chosen in such a way to be consistent with the existence of two flow regimes with opposite anomalies. Here we want to investigate the structure of the low-frequency variability generated by the same model, but with a less arbitrary forcing definition. The purpose of this study is therefore to clarify the role played by the internal quasi-geostrophic dynamics in generating the main low-frequency variability patterns characterising the Northern Hemisphere wintertime mid-latitude flow. We will investigate the modelled variability using a number of well-established diagnostic tools, such as empirical orthogonal functions, teleconnection patterns and blocking indices. Very long integrations (of the order of 100 000 days) will be analysed, in order to investigate variations in circulation statistics occurring on time scales of 10 years or longer which are only due (as in James and James 1992) to internal atmospheric dynamics. Finally, variability patterns obtained in perpetual-winter and seasonal-cycle mode will be compared.

The work is organised as follows. Section 2 contains a brief description of the QG model (the reader is referred to MM93 for more details). Section 3 describes the two model simulations of the wintertime climatology, i.e. the perpetual winter run and the seasonal run. Section 4 deals with the teleconnection patterns found in the model integrations comparing them with reality, while Sect. 5 concentrates on objectively diagnosed blocking and its space–time variability. Section 6 contains a summary and some final conclusions.

2 The quasi-geostrophic model

2.1 Model design

The model is a spectral three level quasi-geostrophic (QG) model (Marshall and Molteni 1993) with global domain and pressure as the vertical coordinate; it integrates prognostic equations for the quasi-geostrophic potential vorticity (PV) at 200, 500 and 800 hPa respectively. The series of spherical harmonics used in the representation of horizontal fields has a triangular truncation at total wavenumber 21 (T21).

The prognostic equation for QG potential vorticity is integrated in the model at the three horizontal pressure levels of 200, 500 and 800 hPa; dissipative and forcing terms are also present in order to represent the effects of diabatic processes, leading to the following prognostic equations:

$$\frac{\partial q_1}{\partial t} = -J(\psi_1, q_1) - D_1(\psi_1, \psi_2) + S_1 \tag{1}$$

$$\frac{\partial q_2}{\partial t} = -J(\psi_2, q_2) - D_2(\psi_1, \psi_2, \psi_3) + S_2 \tag{2}$$

$$\frac{\partial q_3}{\partial t} = -J(\psi_3, q_3) - D_1(\psi_2, \psi_3) + S_3 \tag{3}$$

where the index $i = 1,2,3$ refers to the pressure level. The potential vorticity q is defined as:

$$q_1 = \nabla^2\psi_1 - R_1^{-2}(\psi_1 - \psi_2) + f \tag{4}$$

$$q_2 = \nabla^2\psi_2 - R_1^{-2}(\psi_1 - \psi_2) - R_2^{-2}(\psi_2 - \psi_3) + f \tag{5}$$

$$q_3 = \nabla^2\psi_3 - R_2^{-2}(\psi_2 - \psi_3) + f(1 - h/H_0) \tag{6}$$

where $f = 2\Omega \sin\phi$, $R_1 = (700\text{ km})$ and $R_2 = (450\text{ km})$ are Rossby radii of deformation appropriate to the 200–500 hPa layer and the 500–800 hPa layer, respectively; h is the (realistic) orographic height: and H_0 a scaling parameter for topography (set at 7 km). In Eqs. 1–3, D_1, D_2 and D_3 are linear operators representing the effects of Newtonian cooling, Ekman dissipation on the 800 hPa wind (depending on the underlying surface), and hyperviscosity.

2.2 Forcing

The terms S_1, S_2 and S_3 are time independent but spatially varying sources of potential vorticity which represent the (average) combined effects of diabatic heating and advection by the divergent flow. As suggested by Roads (1987), these can be determined by requiring that, for a climatological ensemble of observed fields, the average potential vorticity tendencies (i.e. time derivatives) computed from Eqs. 1–3 vanish. This condition can be written as:

$$\{-J(\psi, q) - D(\psi)\} + S = 0 \tag{7}$$

where the brackets $\{\ \}$ represent the average over the climatological ensemble, and the index of the vertical level is omitted for simplicity. If $\psi_c = \{\psi\}$ is the observed climatological mean, and a prime denotes a deviation from this mean, Eq. 7 can be rewritten as:

$$-J(\psi_c, q_c) - \{J(\psi', q')\} - D(\psi_c) + S = 0 \tag{8}$$

where the term

$$J' = -\{J(\psi', q')\} \tag{9}$$

represents the contribution of the "transients" on all time scales to the average potential vorticity tendency.

Requiring a null average PV tendency is therefore equivalent to defining S from Eq. 8, where J' is computed using the full range of observed variability. An alternative strategy (used for example in the barotropic instability study by Simmons et al. 1983), is to neglect the term J' completely, and assume that the observed climatology is an exact stationary solution. Such a method represents a sort of zero order truncation in a Taylor expansion of the Jacobian, where the role of the deviations from the mean, which contribute to a large extent to the maintenance of the mean itself, is ignored. In the case of a global (baroclinic) multilevel quasi-geostrophic model, J' cannot be neglected if one wants to reproduce a realistic climatology. It should be pointed out that the model *may* reproduce a mean state equal to ψ_c only if its internal variability is identical (more precisely, if it generates the same J') to the observed variability within the ensemble used for the computation of S.

Since we want to investigate the internal atmospheric dynamics in the absence of forcing anomalies, we should not expect the model to reproduce that part of low-frequency variability which is induced by variations in boundary conditions. Therefore, in the computation of J', a threshold period of N days has been introduced, and only the transients on time scales shorter than this period have been considered. The parameter N has been tuned by comparing the model climate, including high and low frequency variability fields, with observations: an appropriate value for N was found to be 30 days. Such a result suggests, in partial contrast with a number of classical studies which emphasize the role of baroclinic eddies in maintaining the mean flow, that the PV fluxes due to comparatively low-frequency transients are somehow important to produce a good simulation of the atmospheric mean. At the same time, "very low" frequency transients, if they exist, do not appear to influence greatly the mean state of the atmosphere.

The ensemble of observed fields used in the estimates of S_i were ECMWF analyses of stream function at the three pressure levels of the QG model, for each day in January and February 1984 to 1992. Figure 1a shows the barotropic (vertically averaged) component of such a forcing field. The empirical way in which this term has been defined does not allow a straightforward separation of the thermal forcing component from the contribution of other processes. However, the signature of the land-sea contrast and of the storm-tracks can be clearly identified in the forcing for the 800-to-500 hPa layer. To show this, we have taken the difference between the forcing fields at 500 and 800 hPa respectively, and we have removed the zonal mean component. The eddy forcing field so computed is shown in Fig. 1b. It can be noticed that the regions of positive thermal forcing (i.e. positive stream function tendencies) in the northern extratropics are located over the oceans, and particularly in the storm-track regions.

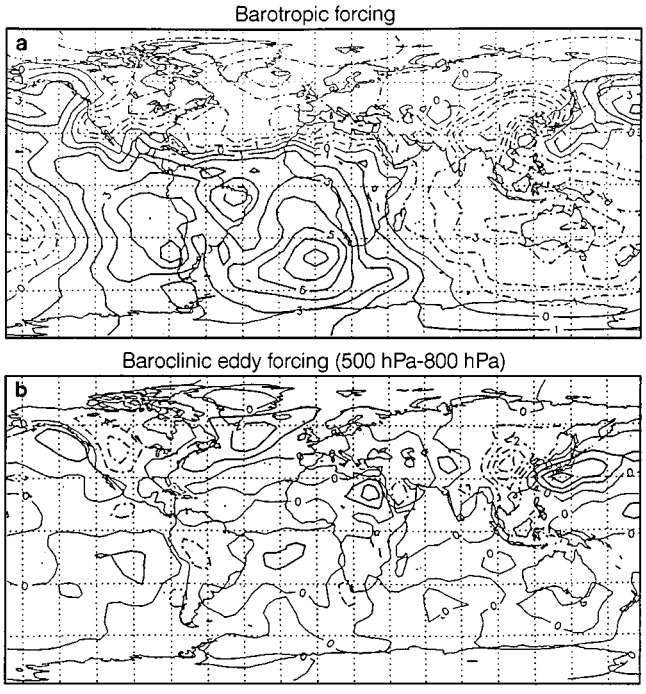

Fig. 1a, b. Model winter forcing. **a** Barotropic component of winter forcing; computed by averaging forcing fields at the 200, 500, and 800 hPa pressure levels; **b** eddy component of the forcing for the 500–800 hPa stream function thickness

3 Simulation of the wintertime climatology

3.1 Perpetual winter run

In the first experiment, a "perpetual winter" integration for 108 000 days (equivalent to 1200 90-day winters) was carried out, driven by the winter, time-independent forcing described above. If the definition of S is appropriate, the quasi-geostrophic model should indeed reproduce the observed wintertime mean state, low-frequency and high-frequency variations of the atmospheric stream function (at least in the northern extratropics) in a realistic way, when a long enough integration is performed.

Figure 2 shows maps of the mean and standard deviation of the 500 hPa stream function from model and observed fields. The standard deviation is shown separately for 5-day mean fields and deviations from 5-days means, in order to evaluate the low-frequency and high-frequency components of the model variability. The observed fields used for comparison are derived from the same dataset used to compute the model forcing.

The simulated mean field pattern is quite realistic, with acceptable errors on amplitude (somewhat underestimated) and phase of the stationary waves. The model distribution of low-frequency variability is very realistic: the three maxima in the North Pacific, North Atlantic and northwestern Siberia are fairly well reproduced, albeit about 10 to 20% lower than observed. However, it must be taken into account that the proportion of low-frequency variability due to interannual variations of surface

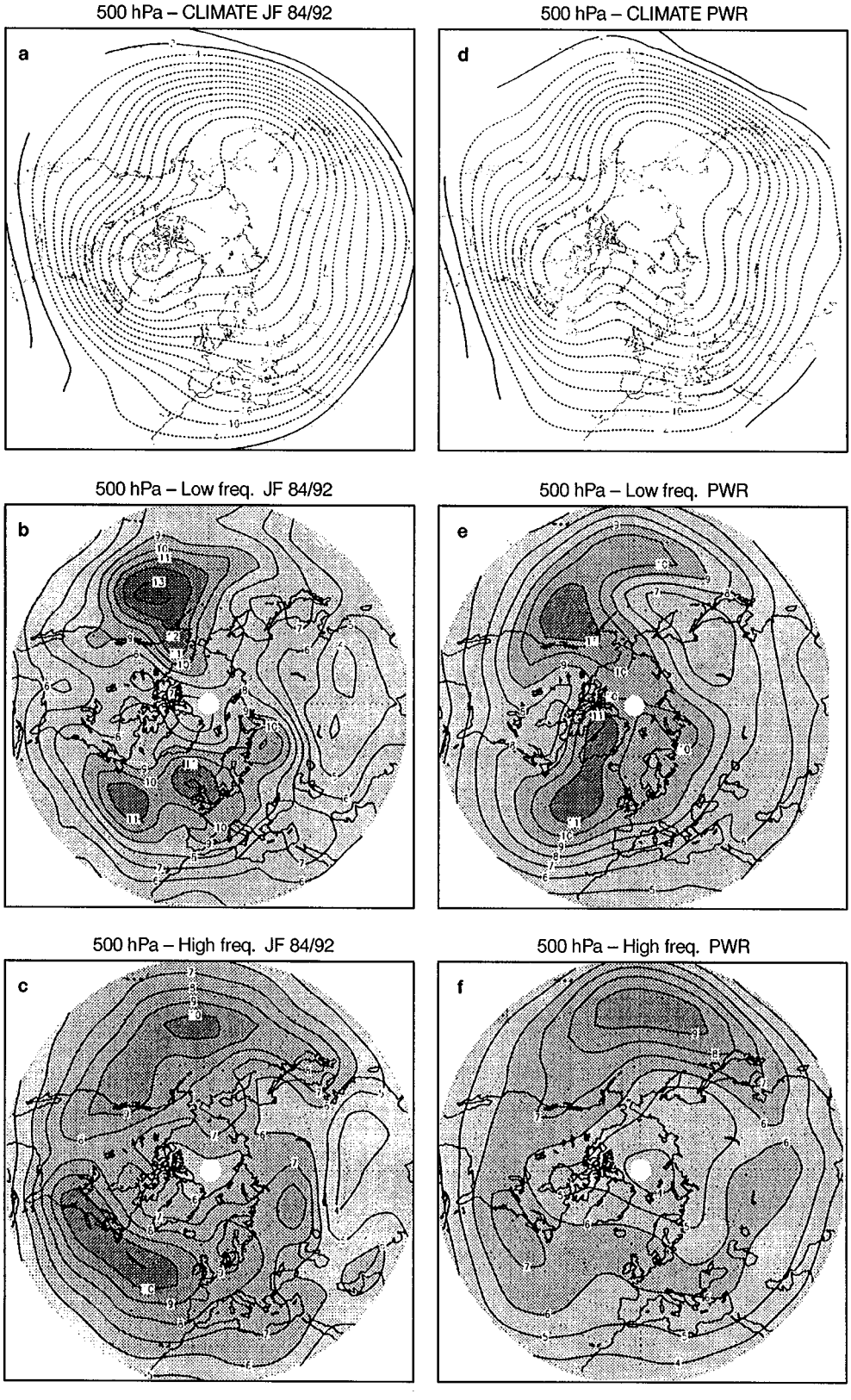

Fig. 2a–f. Statistics of 500 hPa stream function from observed fields in January–February 1884–1992 and from the perpetual winter integration of the QG model. **a** mean field of observations; **b** observed low-frequency standard deviation (computed from 5-days means); **c** observed high frequency standard deviation (from deviations from 5-day means); **d**, **e** and **f**: as in **a**, **b** and **c** from QG model, perpetual winter run

forcing (e.g. SSTs) cannot be simulated by this model. Regarding high-frequency variability, this is of the correct magnitude in the Pacific sector and somewhat underestimated in the Atlantic quadrant.

3.2 Seasonal run

The unrealistic situation characteristic of a perpetual winter could affect the behaviour of the simulated atmo-

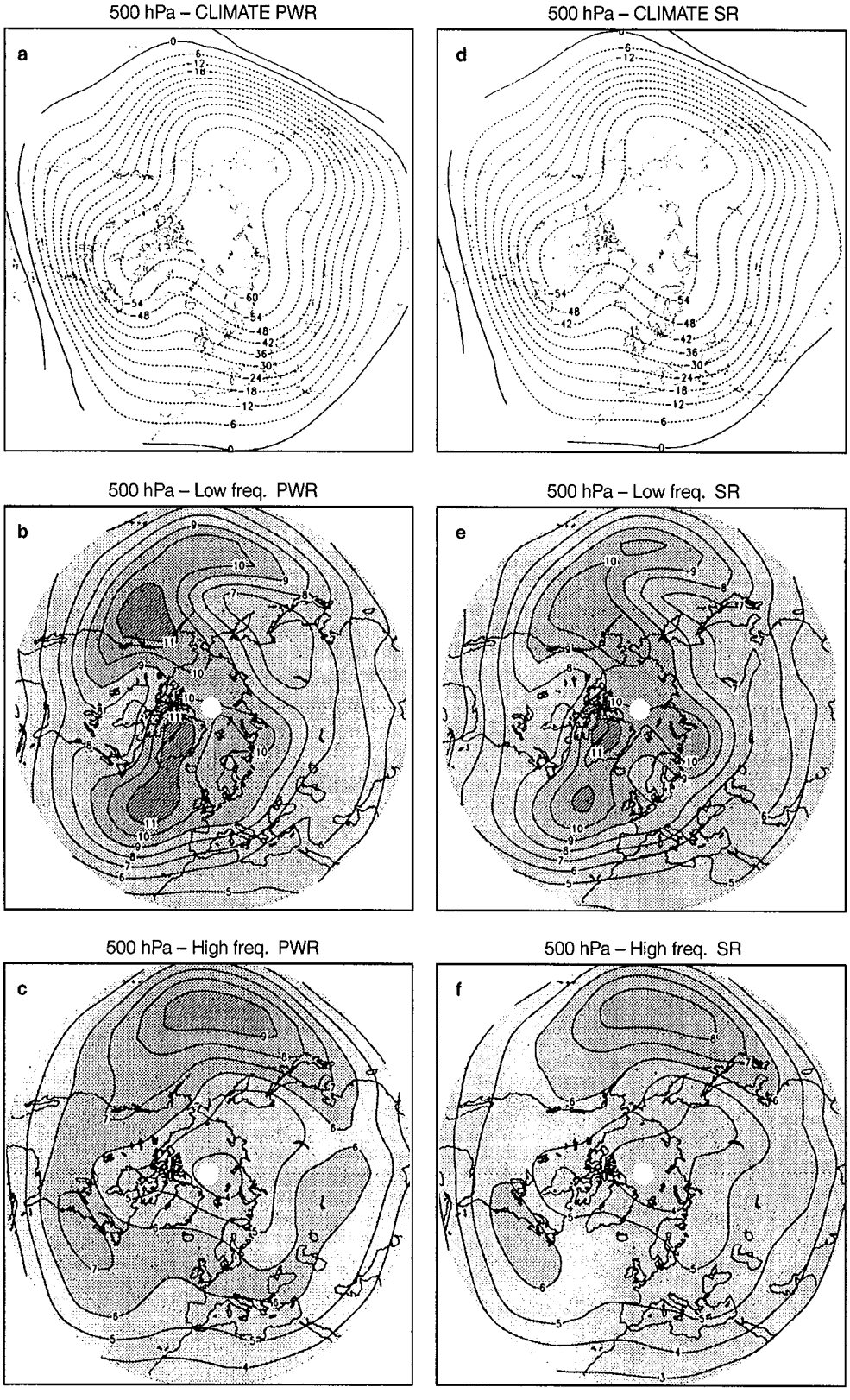

Fig. 3a–f. As in Fig. 2, but **a**, **b**, and **c** for PWR and **d**, **e**, and **f** for SR

spheric circulation. Quasi-stationary states (corresponding to regimes and persistent anomalies) could artificially take root in such a never-ending atmospheric winter flow, and the lack of a seasonal cycle could artificially increase the memory of the system by enhancing the maintenance of quasi-stationary patterns. In order to establish the magnitude of such spurious effects on the low-frequency atmospheric variability patterns found in the "perpetual winter" integration, a "seasonal-cycle" run was carried out.

The seasonal-cycle integration employed a time-dependent forcing field updated daily. Such variable forcing function was obtained by fitting a sinusoidal function (with a 360-day period) between two extreme summer and winter forcings. The winter forcing was the same used for the perpetual winter run, while the summer counterpart was obtained analogously from ECMWF analysis fields of July and August 1984 to 1992. Before carrying out the seasonal integration, a check on the realism of the quasi-geostrophic simulation of the summer season was performed by running the model in perpetual-summer mode (i.e. using the time independent July–August forcing) for a period of 50 summers.

The results of such perpetual-summer run will not be shown here for brevity. It will suffice to say that this simulation was generally much less satisfactory than the winter run, with an acceptable mean summer model climate but with a much underestimated (and spatially unrealistic) variability. This behaviour had, however, to be expected given the limitations imposed by the quasi-geostrophic nature of the model. On the basis of this result, it was decided to extract from the seasonal-cycle run only the three-month winter periods corresponding to January–February–March, and restrict the analysis to such a dataset. In order to make the total length of the extracted winter dataset identical to the duration of the perpetual winter run, the complete seasonal integration was in fact four times longer (1200 12-month years). The rationale behind the performing of two experiments that are *quasi*-identical (same values of all parameters other than forcing, same duration in time) was therefore solely to assess the importance of periodically removing the model atmosphere from its winter state, even if this was done by forcing it towards a rather unrealistic summer.

Figure 3 shows maps of the mean, low-frequency and high-frequency variability of the 500 hPa stream function from the perpetual winter run (PWR hereafter) and seasonal run (SR hereafter) output fields. The main features of the two winter climates and variability patterns appear to be very similar; at least for such general aspects, the seasonal simulation appears as good as the perpetual winter one. From such a brief comparative analysis of the PWR and SR (winter only) integrations it would appear as if the influence of the simulated seasonal cycle on the main features of the model atmosphere is rather small. A more detailed analysis of the low-frequency variability patterns of both integrations will be described in the next sections.

4 Low-frequency variability patterns

Two classical approaches to the study of low-frequency variability will be presented in this section. First of all, we will analyse teleconnection patterns defined by one-point correlation maps; in defining them we refer here to Wallace and Gutzler's (1981; WG81 hereafter) seminal work. We will then describe and compare the results of empirical orthogonal function (or principal component) analysis.

4.1 One-point correlation (teleconnection) maps

One-point correlation maps of stream function anomaly on the 500 hPa pressure level were calculated for all points belonging to the Northern Hemisphere gaussian grid of the T21 QG model (1024 points in all). Such calculations were carried out on the output of both the PWR and SR integrations. The model's one-point correlation maps were subsequently compared to observed one-point correlation maps, recomputed from 500 hPa geopotential height fields using the same procedure as in WG81. For this analysis, the observational dataset was obtained by merging NMC data for the period 1949-to-1980 with ECMWF data for the period 1981–1992, after having transported both original datasets on a common $3.75^\circ \times 3.75^\circ$ regular lat.–lon. grid.

For the PWR run, anomaly fields used in the construction of one-point correlation maps were computed by subtracting the climate of the entire run from 90-day means, where 90 consecutive days can be considered as a winter season. As far as the SR run is concerned, in which the empirical forcing is time-dependent, we first computed winter anomalies in the same way as for the PWR run, i.e. by subtracting the model winter climate (recomputed from the SR run) from seasonal averages. We then separately recalculated correlation maps for the first and the second 45-day period of each winter season, in order to investigate if the structure of the teleconnections changed during the transition period between winter and spring. Since no significant difference was observed in SR teleconnections referring to the first and second half of the winter season, only teleconnection maps relative to the entire winter season will be shown here, as for the PWR run.

A well-defined pattern, shown in Fig. 4, frequently recurrs in the model teleconnection maps. This pattern is characterized by the presence of five centres of action, located on a latitudinal belt around latitude 40 °N, positively correlated with each other, and negatively correlated with the high latitudes, around 60 °N. Even though this signal was found to be quite strong, it was possible to further identify a clear signature of the two best-known teleconnection patterns, i.e. the North Atlantic Oscillation (NAO, corresponding to the eastern Atlantic pattern in the 500 hPa analysis of WG81), and the Pacific/North American (PNA) pattern. The base points that best represent these two teleconnection patterns, both in the observation and in the model simulations, are reported in Tables 1 (NAO) and 2 (PNA).

Correlation maps for base points NAO(a) and PNA(a) of both integrations are shown in Fig. 5, where they are compared to their observed counterpart. The main features of the model's teleconnections with respect to observed teleconnections, are the following:

1. The centres of action of the NAO are measurably shifted westward with respect to one-point correlation maps obtained from observed data, i.e. the NAO is shifted towards the North American continent (we will show later that this is consistent with a comparable shift of the Atlantic blocking sector).
2. The model centres of action of the PNA pattern cover a slightly wider area in longitude, especially in the PWR run; base point PNA(a) is located near its observed counterpart, in the tropical Central Pacific, while base

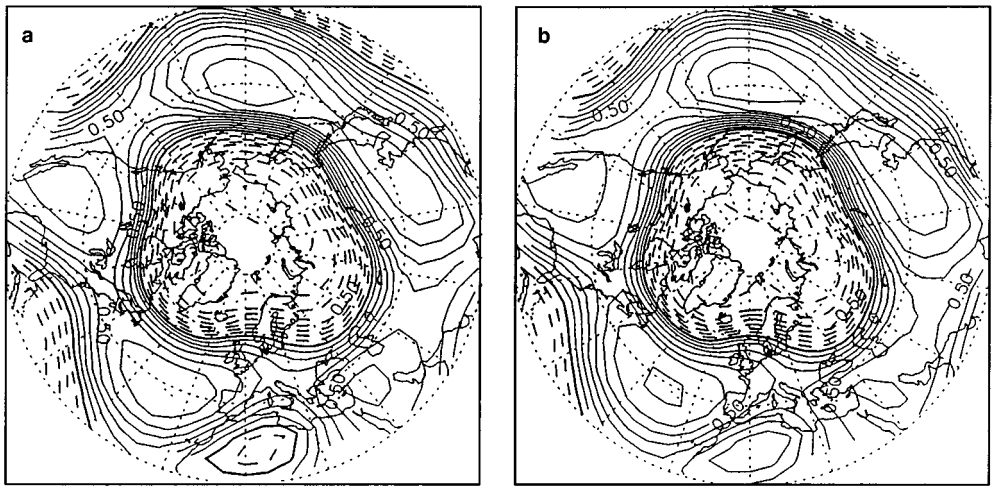

Fig. 4a, b. One-point correlation map for point (42 °N, 180 °E) of **a** PWR and **b** SR

Table 1. North Atlantic Oscillation

NAO	Observed data	PWR run	SR run
NAO(a)	(26 °N, 26 °W)	(19 °N, 34 °W)	(25 °N, 39 °W)
NAO(b)	(56 °N, 19 °W)	(53 °N, 45 °W)	(53 °N, 45 °W)
NAO(c)	(49 °N, 41 °E)	(36 °N, 17 °E)	(36 °N, 17 °E)

Table 2. Pacific/North American pattern

PNA	Observed data	PWR run	SR run
PNA(a)	(22.5 °N, 161 °W)	(19 °N, 157 °W)	(19 °N, 157 °W)
PNA(b)	(45 °N, 165 °W)	(53 °N, 141 °W)	(53 °N, 152 °W)
PNA(c)	(56 °N, 116 °W)	(58 °N, 96 °W)	(58 °N, 101 °W)
PNA(d)	(30 °N, 86 °W)	(30 °N ,67 °W)	(25 °N, 79 °W)

points PNA(b), PNA(c), and PNA(d) are moved eastward, with respect to their observed counterparts.

Therefore the entire PNA pattern appears to be shifted eastwards, while the NAO is shifted in the opposite direction. As a consequence, it becomes difficult to separate the signatures of NAO and PNA in the region covering the western Atlantic Ocean and the eastern coast of the North American continent. This can be best observed in Fig. 6, where correlation maps corresponding to base point PNA(d), located at (30 °N, 67 °W) in PWR and at (25 °N, 79 °W) in SR, are shown. In these two maps the contributions of both teleconnection patterns clearly overlap.

4.2 Empirical orthogonal function analysis

The leading variability patterns of the model atmosphere were also independently searched for by calculating empirical orthogonal functions (EOFs) of daily 3-level stream function anomalies from both integrations. In performing such calculations, EOFs were normalised using total energy. The cumulative variance explained by the first 30 EOFs is only 43% of the total in the PWR and 45.5% in the SR (the variance of each component is shown in Fig. 7), but it must be remembered that here the total variance includes both low-frequency and high-frequency contributions from all three model vertical levels. In fact, when the same calculations are repeated on PWR fields averaged with a 10-day running mean, the variance explained by the first 30 EOFs increases to 63%.

Figure 8 shows the first five EOFs at the 500 hPa level of the perpetual winter run. A wavenumber-five eddy field superimposed to a strong zonal-mean profile characterizes EOF 1; it may be noticed that this pattern very closely resembles the recurrent hemispheric pattern found amongst one-point correlation maps (shown in Fig. 4). It is also possible to recognise in EOFs 4 and 5 the NAO and PNA teleconnection patterns previously described. EOFs 2 and 3 are most likely representative of baroclinic transient waves: in fact, these EOFs disappear if the analysis is performed from 10-day mean fields (not shown).

The leading EOFs of SR stream function anomalies are shown in Fig. 9 at the 500 hPa level. SR EOF 1, which has no counterpart in PWR, is attributable to the presence of the periodically variable seasonal forcing. SR EOF 2 exhibits the same structure as the PWR EOF 1, while the NAO and the PNA are represented respectively by EOFs 5 and 6. EOFs 3 and 4 are comparable with the previous PWR EOFs 3 and 2.

It is important to stress that the two main teleconnection patterns characterising the Northern Hemisphere wintertime mid-latitude flow (NAO and PNA), have been found in simulations produced by a simple quasi-geostrophic model with no time-varying diabatic energy source, using two different diagnostic methods. Our results suggest that both teleconnections can be interpreted as preferred "internal modes" of oscillation of the extratropical atmosphere in the low-frequency variability range (cf. Lau 1981).

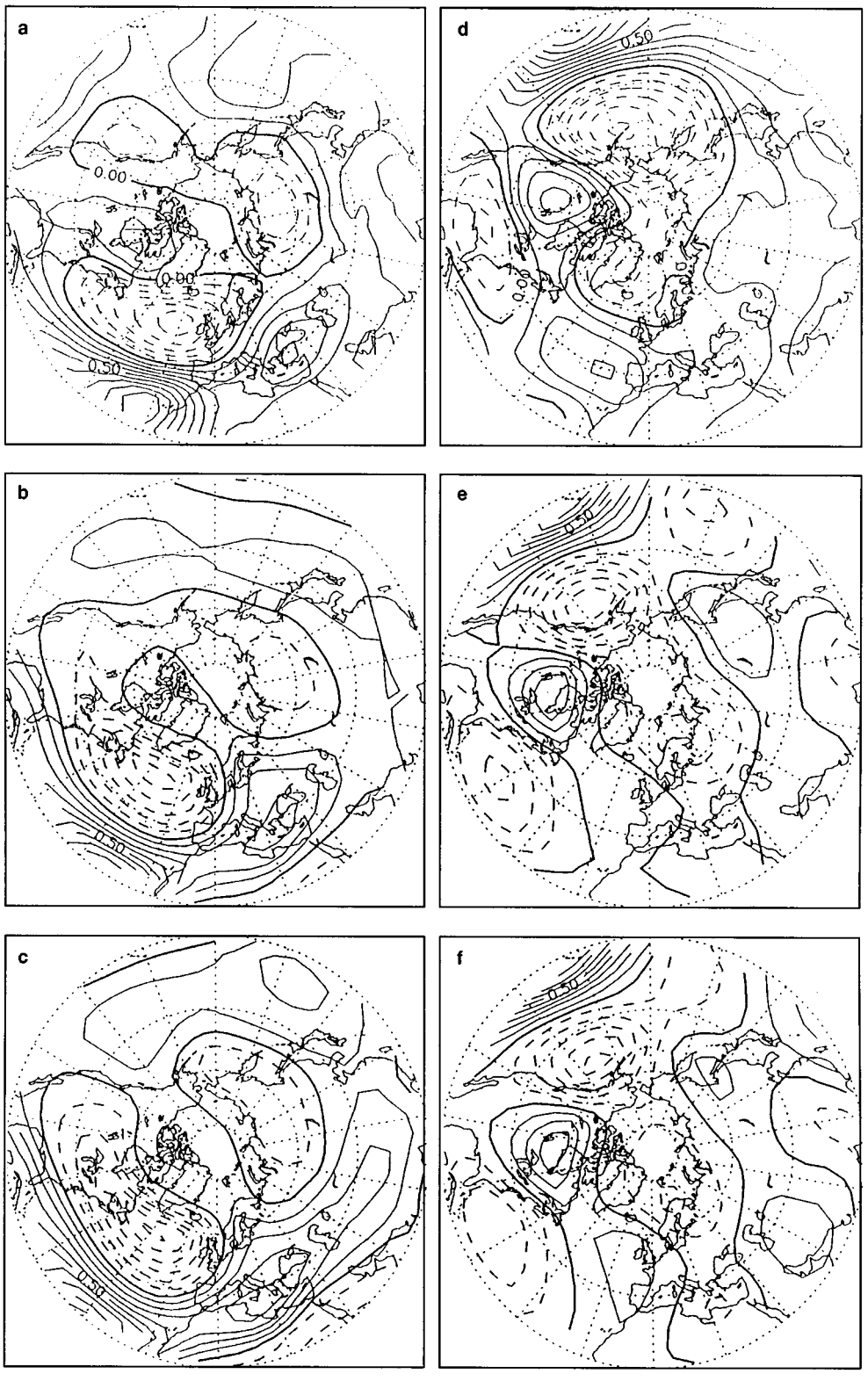

Fig. 5a–f. One-point correlation maps. Point NAO **a**, centred at: **a** (26 °N, 26 °W) in observations, **b** (19 °N, 34 °W in PWR, and **c** (25 °N, 39 °W) in SR. Point PNA (a), centred at: **d** (22.5 °N, 161 °W) in observations, **e** (19 °N, 157 °W) in PWR, and **f** (19 °N, 157 °W) in SR

5 Atmospheric blocking

5.1 Blocking index

Simulation of blocking events in the model atmosphere was investigated using the Tibaldi and Molteni's blocking index (Tibaldi and Molteni 1990, hereafter TM90). The blocking index was slightly modified with respect to the original definition given in TM90, since the comparison of observed fields objectively classified as blocked showed a better agreement with subjective classifications based on synoptic experience.

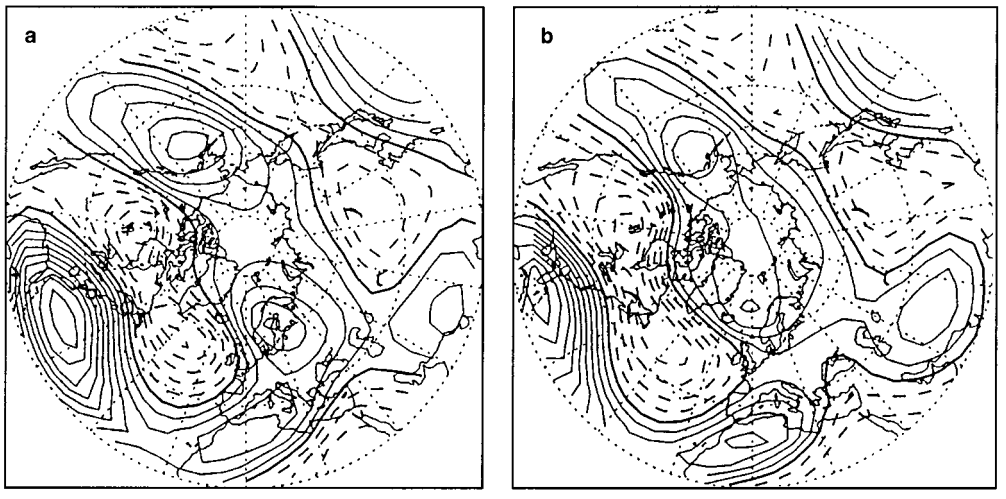

Fig. 6a, b. One-point correlation maps, relative to point PNA(d), located at **a** (30 °N, 67 °W) in PWR, and at **b** (25 °N, 79 °W) in SR

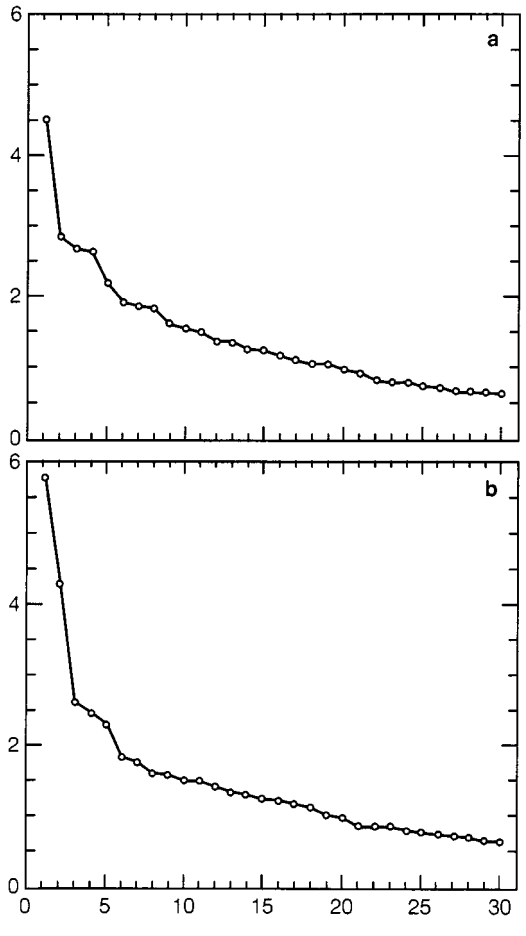

Fig. 7a, b. Variance explained by the first 30 EOFs: **a** PWR; **b** SR

In defining TM2 blocking indices geopotential height gradients GHGS and GHGN was computed for each longitude point of the grid:

$$GHGS = \frac{Z(\phi_0) - Z(\phi_S)}{\phi_0 - \phi_S} \tag{10a}$$

$$GHGN = \frac{Z(\phi_N) - Z(\phi_0)}{\phi_N - \phi_0} \tag{10b}$$

where

$\phi_N = 80\,^\circ N + \Delta,$

$\phi_0 = 60\,^\circ N + \Delta,$

$\phi_S = 40\,^\circ N + \Delta,$

$\Delta = -4^\circ, 0^\circ$ or 4°.

A given longitude was defined as 'blocked' at a specific instant when the following two conditions were satisfied for at least one value of Δ:

$$GHGS > 0 \tag{11a}$$

$$GHGN < -5 \text{ gpm}/^\circ\text{lat}. \tag{11b}$$

Condition 11a, equivalent to Lejenäs and Økland's criterion (Lejenäs and Økland 1983) is a requirement for the prevailing westerly zonal flow to be 'reversed', i.e. for the flow to be zero or easterly, at mid-latitudes. Condition 11b is satisfied in the presence of a not-weaker-than-average westerly current at higher latitudes. Both conditions, when simultaneously satisfied in a longitudinally extended region, allow to identify a 'blocking high' configuration approximately positioned around 60 °N.

Figure 10 shows the distribution (as a function of longitude) of the frequency of occurrence of conditions 11a and 11b (Fig. 10b and c respectively) and of the TM2 index (Fig. 10a), computed from the observed dataset described in Sect. 4.1.

Because at high latitudes westerlies have a climatological maximum in the Euro-Atlantic region, condition 11a is usually sufficient to identify blocking configurations in

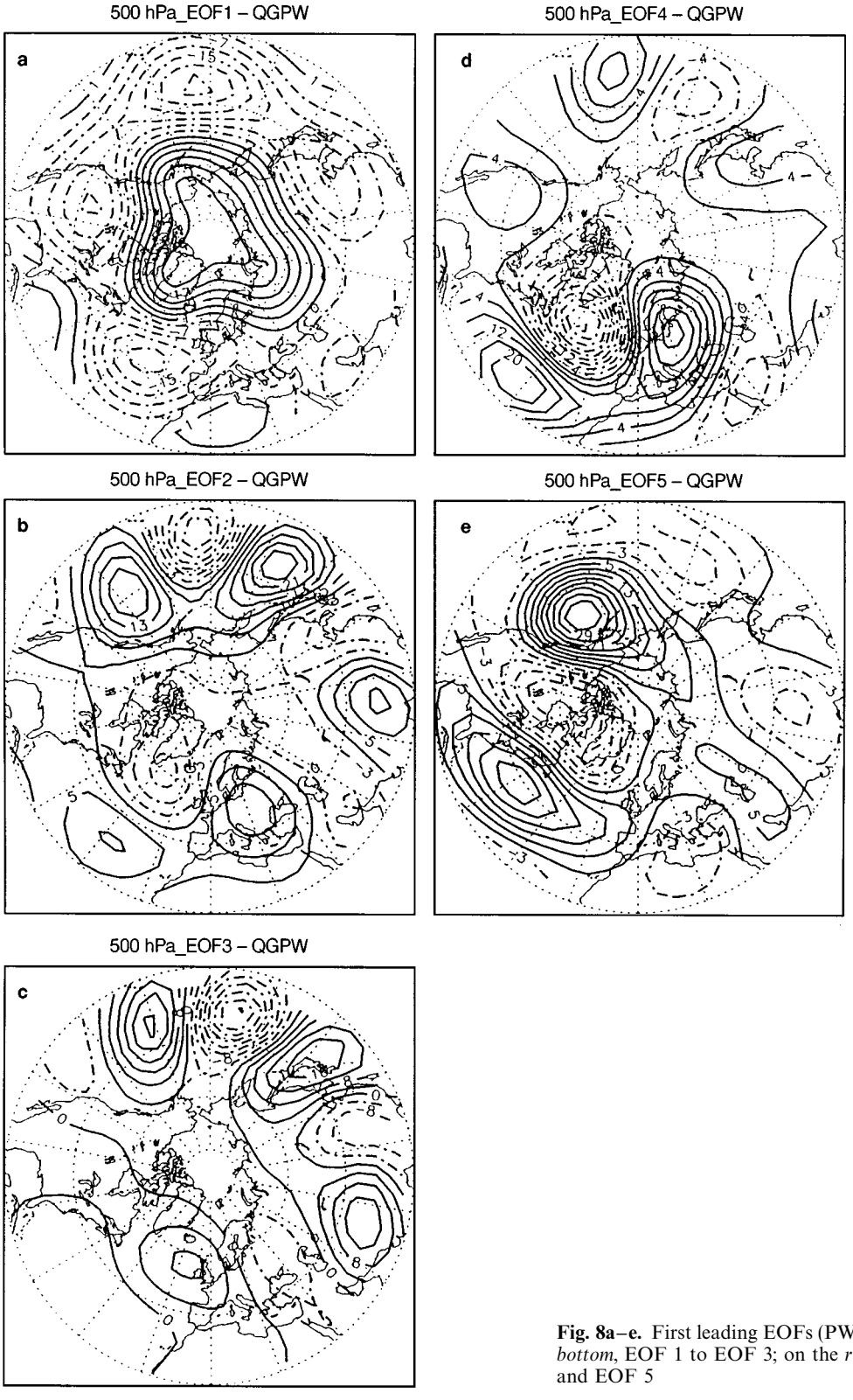

Fig. 8a–e. First leading EOFs (PWR) at 500 hPa level: *on the left*, *top to bottom*, EOF 1 to EOF 3; on the *right*, *top to bottom*, EOFs 4 and EOF 5

this region, since condition 11b is satisfied in approximately 70% of winter days in the observed climatological record. This is not the case in the Pacific region; condition 11b has a marked frequency minimum around 140 °E of longitude, i.e. at the western limit of the Pacific sector, and attains a relative maximum at 130 °W, i.e. at the eastern limit of the Pacific ocean. Therefore condition 11b plays a fundamental role in discriminating between blocked

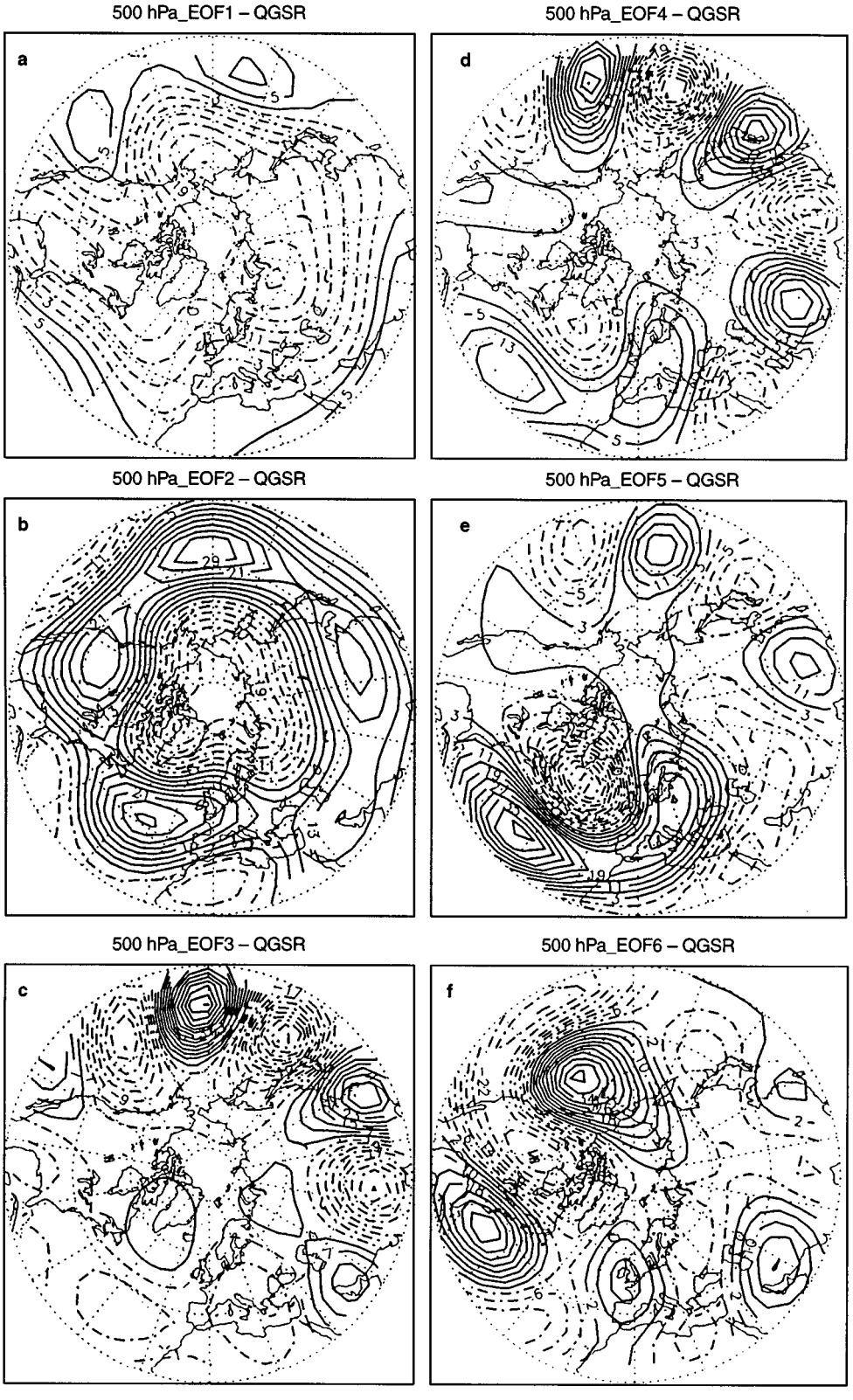

Fig. 9a–f. First leading EOFs (SR) at 500 hPa level: *on the left*, *top to bottom*, EOF 1 to EOF 3; on the *right*, *top to bottom*, from EOF 4 to EOF 6

configurations and cut-off lows in the Western Pacific region. It follows that the number of configurations counted as blocked by TM2 in this region is substantially lower when compared to the same number obtained using Lejenäs and Økland's (1983) criterion.

Conditions 11a and 11b were subsequently adapted to stream function values to be used in the QG model framework. While condition 11a remains unchanged, condition 11b needs to be scaled to stream function values using the linear balance assumption.

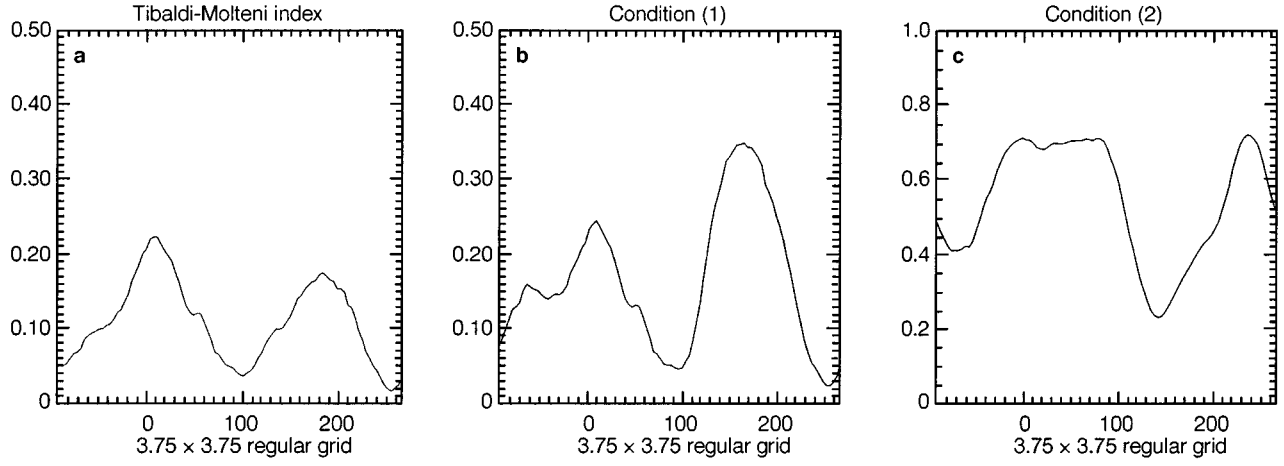

Fig. 10. **a** Blocking frequency diagram for 43 winters of observed 500 hPa geopotential height data analysed with TM2; **b** and **c** conditions (11a) and (11b) of TM2, respectively, for the same observed dataset as above

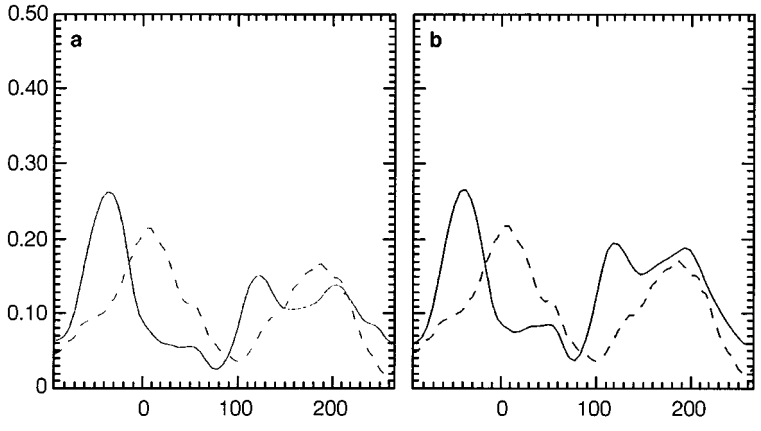

Fig. 11a, b. Blocking frequency diagram for the entire **a** PWR and **b** SR integrations

5.2 Blocking frequency

The longitudinal distribution of blocking frequency according to the TM2 index was calculated from the 1200-winter samples corresponding to the entire PWR and SR simulations (see Fig. 11). The longitudinal dependency of blocking frequency was found to be quite stable within each run when diagrams obtained in different 100-winter periods were compared, thereby allowing us to define 'sectors' where blocking episodes are most likely to occur. These blocking sectors are approximately positioned, in the model as well as in the observed atmosphere, over the eastern Atlantic and Pacific basins, and are consequently termed 'Euro-Atlantic' and 'Pacific' sectors, respectively.

When compared with observed blocking frequency from the 43-winter dataset, the modelled blocking frequency exhibits some interesting differences, for both PWR and SR integrations. In both runs, the Atlantic blocking sector of the model is measurably shifted westwards, of about 30°–40° of longitude (compare solid and dashed lines in Fig. 11). The peak of maximum frequency is well defined, and positioned around 30 °W, with a secondary plateau located eastwards (from 20 °E to 50 °E), more evident in SR. Therefore, the Atlantic blocking sector was defined in the model as comprising the longitudes from 70 °W to 0 °E.

The Pacific sector is harder to delimit, being broader in width. Blocking frequency diagrams exhibit a relative minimum, more pronounced in PWR than in SR, between two maxima (rather than showing one single maximum as observed). The minimum is positioned around 160 °E, with maxima around 120 °E and 160 °W, in PWR; and around 140 °E, with maxima around 120 °E and 170 °W, in SR. The presence of such a minimum in the Pacific region suggested a division of the sector into two subsectors, hereafter called Pacific1 and Pacific2, and respectively defined as ranging from 100 °E to 160 °E , and from 160 °E to 130 °W .

Composite anomaly maps for each subsector were obtained by subtracting the model climate from the average stream function in blocked days. The composite map for subsector Pacific2 closely resembles its observed counterpart, both in position and in shape of positive and negative anomalies (see later). On the other hand, the position and shape of anomalies in the composite for subsector

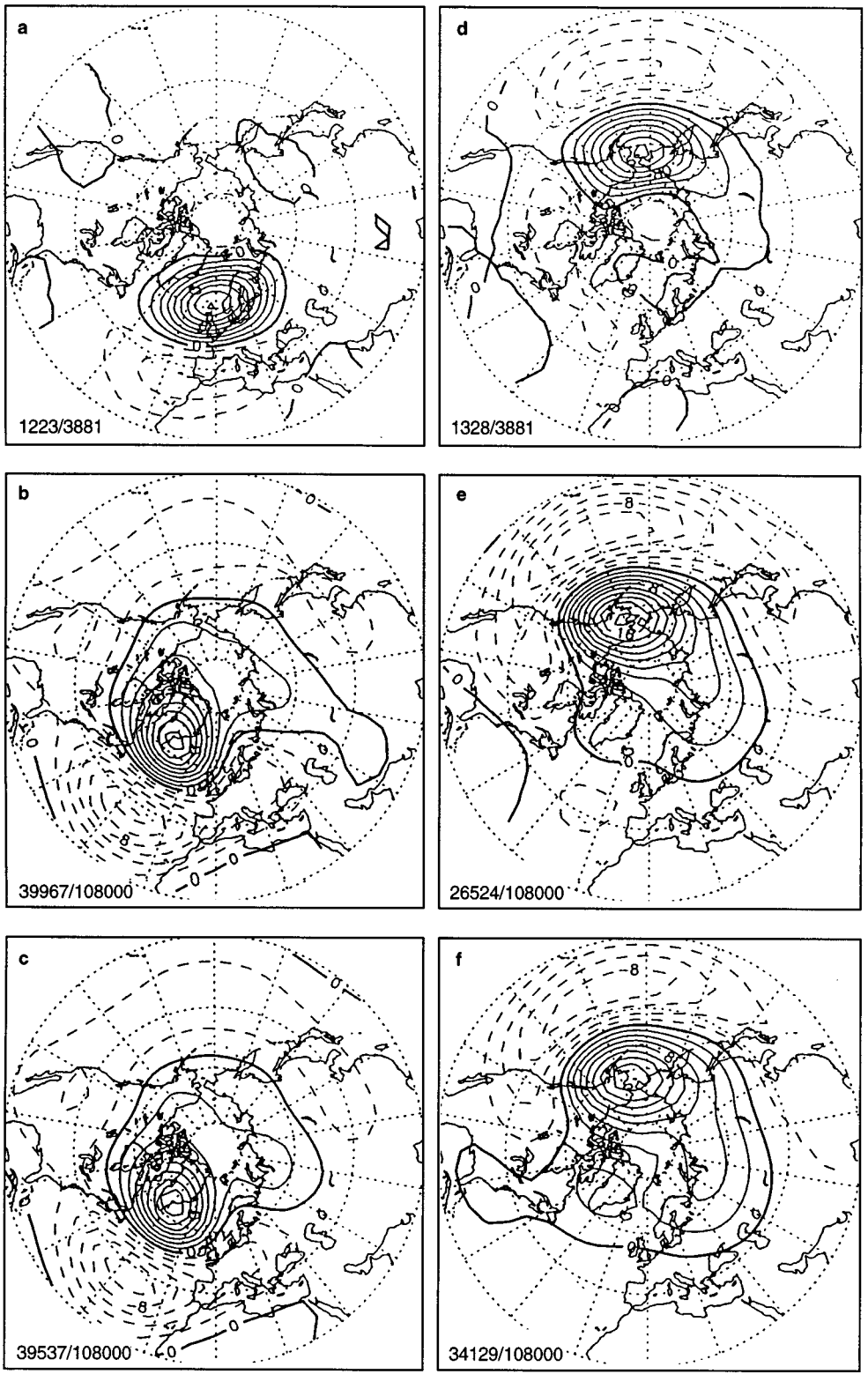

Fig. 12a–f. Composite anomaly maps of blocked days with respect to the entire period analysed: **a** Atlantic blocking in 43 winters of observed 500 hPa geopotential height data. **b** Atlantic blocking in PWR. **c** Atlantic blocking in SR. **d** Pacific blocking in the same dataset as in **a**. **e** Pacific blocking in PWR. **f** Pacific blocking in SR

Pacific1 are not well defined, and this composite has no clear counterpart in the observations. Therefore, from now on, we shall refer to subsector Pacific2 as the Pacific sector as far as model data are concerned.

5.3 Blocking in the Atlantic and Pacific sectors

Characteristics of blocking episodes were further investigated in the Atlantic and Pacific sectors defined already.

Each daily map is catalogued as blocked, in one or both sectors independently, when at least three consecutive longitudes, in that sector, are 'blocked'. Anomaly composite maps of blocked days with respect to the climate of the entire 1200-winter period are shown in Fig. 12 for both the PWR run and the SR run, where they are compared to their observed counterpart. The spatial patterns of Pacific blocking anomalies are well reproduced both in the perpetual-winter and seasonal simulation; for the Atlantic, the centres of the anomaly dipole show a westward shift of 30° probably due to a reduced baroclinic activity in the model simulation of the Atlantic storm track (see Fig. 2c and f). Recent observational studies (V. Pavan, personal communication) show in fact that west Atlantic blocking (well-reproduced by the QG-model) is linked to the negative phase of the North Atlantic Oscillation, while the frequency of the European blocks (underestimated by the model) is strongly related to the number of Atlantic storms upstream of the target region.

The frequency maximum (i.e the frequency corresponding to the longitude of the peak), the mean and standard deviation of the number of blocked days in the sectors, and the average duration of blocking episodes in the two runs are reported in Tables 3 and 4, for the Atlantic and Pacific sectors respectively, where they are compared to the observed climatology in the 43-winter sample.

Blocking activity in the Atlantic sector is substantially stable in passing from PWR to SR; the overestimation in the longitudinal frequency maximum is compensated by the underestimation of blocking frequency in the European region (see again Fig. 11), so that the number of blocked days in the whole sector is only 15% higher than the observed value. Interestingly, the interannual variations of such numbers are at least as strong in the model as in the analysis, despite the absence of interannual variations in the forcing.

Table 3. Atlantic blocking, (70 °W, 0 °E)

	Observations	PWR	SR
Maximum blocking frequency (%)	22.3	27.3	27.3
Blocked days per winter	28.3 ± 10.4	33.3 ± 13.5	32.9 ± 14.7
Mean duration of episodes (days)	10.5	11.9	12.0

Table 4. Pacific blocking, (160 °E, 130 °W)

	Observations	PWR	SR
Maximum blocking frequency (%)	17.5	14.4	19.2
Blocked days per winter	30.7 ± 12.3	22.1 ± 9.5	28.4 ± 11.2
Duration of episodes (days)	10.8	8.9	9.9

Table 5. Number of blocked days per 45 days

	SR: first half	SR: second half
Atlantic	17.4	15.6
Pacific	12.0	16.4

As far as the Pacific sector is concerned, a substantial increase in blocking activity can be noticed from PWR to SR; the statistics are much closer to the observed ones for the latter integration. When blocking statistics in the SR run are recomputed by dividing each winter into two periods of 45 days each (corresponding to January and March conditions respectively) one finds that the increase in Pacific blocking region is concentrated in the second half of the winter season (see Table 5).

To investigate the possible mechanisms that lead to such a change, mean and standard deviations of stream function were separately re-calculated for the first and second half of the winter seasons belonging to the SR (SR1 and SR2 respectively hereafter). As shown in Fig. 13, SR1 has a stronger westerly flow in midlatitudes (particularly in the Pacific blocking sector, 160 °E, 130 °W) and a larger

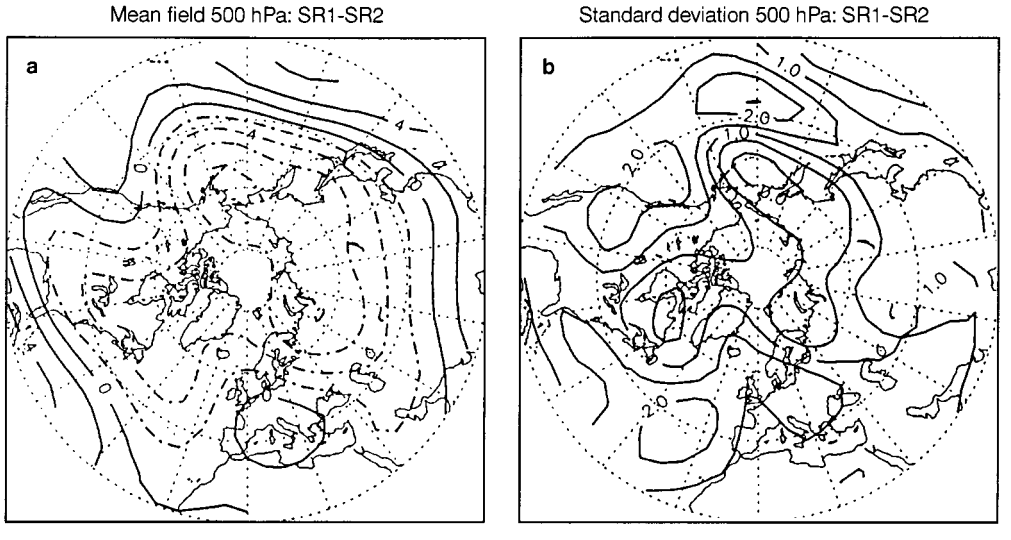

Fig. 13a, b. Statistics of 500 hPa stream function: **a** difference between SR1 and SR2 mean fields; **b** as in **a** for the standard deviations

variability (the largest differences being over the midlatitude oceans). Since stronger westerlies tend to oppose the occurrence of blocking episodes, while stronger variability is usually associated with more blocks, it seems that the increase in Pacific blocking activity from SR1 to SR2 is attributable to changes in the mean flow, rather than in the variance of the flow itself.

In order to determine with more accuracy the role played by the seasonally varying mean state (i.e. by January rather than March conditions), as compared to the role played by the change in variability, two artificial datasets were created in which the mean and variance of the two half-seasons were exchanged. A stream function (ψ) field belonging to the i-th 45-day period, with $i = 1, 2$, can be written as

$$\psi(i) = \{\psi(i)\} + \psi(i)' \tag{12}$$

where the brackets $\{\ \}$ represent the climatological average and the prime ($'$) denotes the anomaly. By exchanging the mean states between the two half-samples, we define:

$$\tilde{\psi}(1) = \{\psi(2)\} + \psi(1)' \tag{13}$$

$$\tilde{\psi}(2) = \{\psi(1)\} + \psi(2)' \tag{14}$$

where by construction the $\tilde{\psi}(i)$ fields have the same standard deviation as the $\psi(i)$ with the same subsample index.

Longitudinal distributions of blocking frequency calculations were re-computed from the two original and the two artificial subsamples, and are shown in Fig. 14. The results of this experiment are as follows:

1. For the original data, as indicated in Table 5, blocking frequency is significantly higher in the Pacific region during SR2 than during SR1 (Fig. 14a and b), while it is slightly lower in the Atlantic;
2. When mean states are exchanged, Pacific blocking frequency increases in the $\tilde{\psi}(1)$ dataset with respect to $\psi(1)$ (compare Fig. 14a and c), while it decreases in the second 45-day period $\tilde{\psi}(2)$, (compare Fig. 14b and d); among the two artificial datasets, the sample with the mean state of SR2 and the variance of SR1 is the one with the largest blocking frequency in the Pacific;
3. Comparing Fig. 14a to d and Fig. 14b to c respectively, one can consider the same blocking frequency diagrams also in terms of an exchange of transients. Such an exchange can also be seen to yield a change in Pacific blocking frequency, but of smaller magnitude. (Pacific blocking frequency in Fig. 14 c is higher than in Fig. 14d);
4. Conversely the decrease of Atlantic blocking frequency in passing from SR1 to SR2 is completely due to a change in the eddy component of the flow (Atlantic blocking frequency is higher in Fig. 14a than in d, lower in Fig. 14b than in c; while no changes are found when climates are exchanged).

The results of this analysis confirm that the increase of blocking activity in the Pacific region during the seasonal integration is primarily due to a change in the mean flow, rather than in the variance of the flow itself. The mean flow does change in passing from an average-January to an average-March condition as a response to the

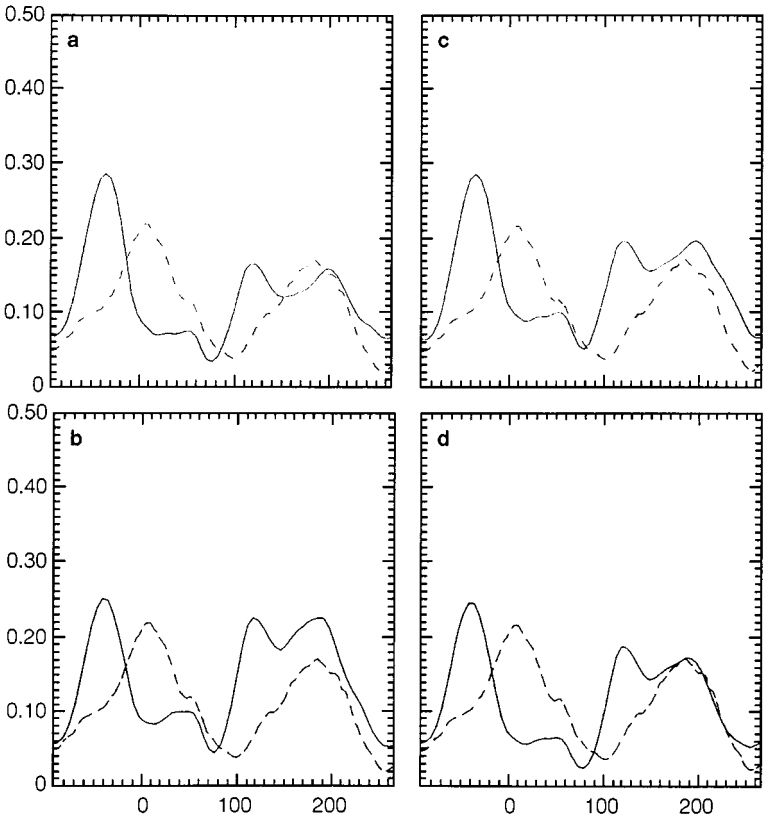

Fig. 14a–d. Blocking frequency diagrams: **a** in the first 45-day period of SR, **b** in the second 45-day period of SR, **c** in the first 45-day period of SR, with climate of the second 45-day period, **d** in the second 45-day period of SR, with climate of the first 45-day period. See text for more exhaustive explanations

seasonally-varying forcing term. As shown in Fig. 13, the modelled westerly jet is reduced (at it should be) from the first to the second half of the winter season; the SR1-minus-SR2 map has a significant centre of negative difference in the North Pacific, approximately positioned around 180 °E. It is plausible that this weakening of the westerlies makes it easier for the flow to verify condition (11a) of the Tibaldi-Molteni blocking index.

5.4 Persistence: length of blocking episodes

As pointed out by Rex (1950), a situation of blocked flow at midlatitudes is characterised not only by its peculiar synoptic configuration, but also by the persistence of the flow anomaly on a time scale ranging from a few days to a few weeks.

Durations of blocking episodes were obtained by 'filling in' series of blocking indices for each sector according to the following rule: a non-blocked day followed/preceded by three blocked days, and preceded/followed by at least one blocked day was assumed to have been erraneously defined as non blocked, and counted as blocked. Blocking episodes of duration less than five days were subsequently eliminated from the record.

Distributions of blocking duration in the PWR and SR runs and in the analyses are shown in Fig. 15. The model distributions, for both runs and blocking sectors, have an exponential nature which agrees fairly well with the observed distribution.

The average duration of blocking episodes in the Atlantic sector is very similar in the two model runs, namely 11.9 days in PWR and 12.0 days in SR. In this sector, it is approximately 1.5 days longer than in observed data over

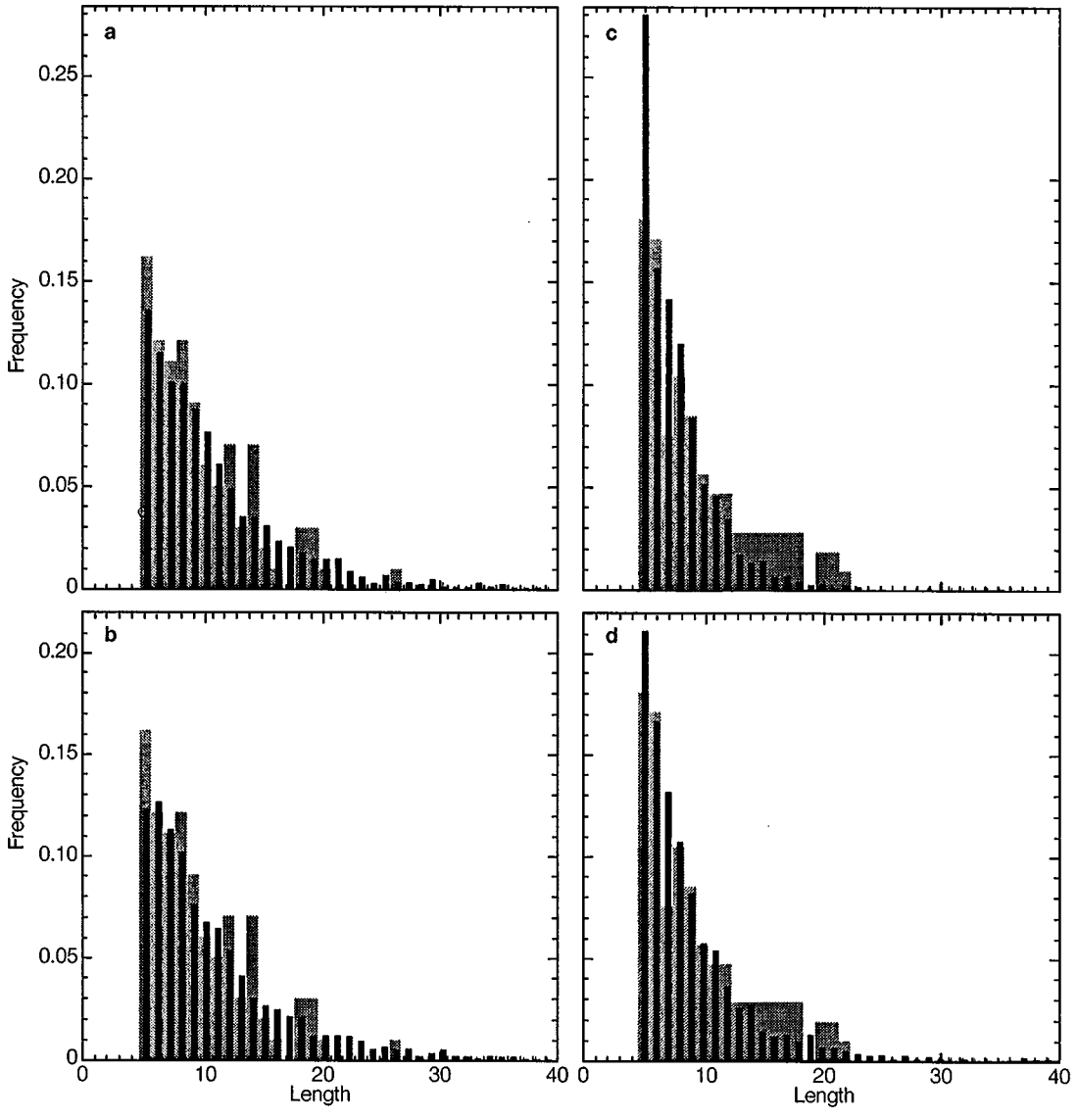

Fig. 15a–d. Distribution of blocking duration (only episodes longer than four days are considered); lighter bars represent the frequency of blocking episodes in the observed dataset, darker bars represent modelled episodes for: **a** Atlantic blocking in PWR. **b** Atlantic blocking in SR. **c** Pacific blocking in PWR. **d** Pacific blocking in SR

the 43 winters considered (10.5 days). This is in partial disagreement with the results of Liu and Opsteegh (1995). Using a different blocking index on a perpetual-winter integration of the same QG model, they found that the model underestimated the duration of Atlantic blocking by 1.2 days (the observed duration being 9.3 days, versus 8.1 days in the model). In the Pacific sector, blocking duration is underestimated by the model with respect to observed data, both in PWR and in SR. Consistently with the behaviour of blocking frequency, an increase can be noticed from PWR (8.9 days) to SR (9.9 days), to be compared with 10.8 days in observed data.

It is worth noting the presence of blocking episodes of duration greater than 20 days in both runs of the model, and in both sectors.

5.5 Interannual and interdecadal variability

Blocking activity in the QG model exhibits a considerable amount of variability on time scales shorter than 50 model winters. Figure 16 displays distributions of winters as a function of number of blocked days per winter, in the Atlantic and Pacific sectors respectively, in the two runs. The number of blocked days per winter varies from five days to 80 days in the Atlantic sector, and from five days to 65 days in the Pacific sector. PWR distributions (Fig. 16a, b) are sharper than SR distributions (Fig. 16c, d), pointing out that an enhanced interannual variability is found when the seasonal cycle is considered.

The decadal variability of blocking activity was investigated computing time series of 10-winter means of number of blocking days per winter for both runs and sectors. Results are summarised in Table 6, while Fig. 17 shows the four time series obtained. As testified by the standard deviation values in Table 6, the QG simulations exhibit a considerable (and realistic) decadal blocking variability, completely attributable to the internal dynamics of the model atmosphere. Strongly blocked decades can be noticed in both integrations: for example the 64th decade of SR exhibits a mean of 45 blocked days per winter in the Atlantic sector, while the 71st decade of SR reaches the mean of 38 blocked days per winter in the Pacific sector. Zonal decades can be found as well, with a mean of only 23 blocked days per winter (76th decade in SR) for the Atlantic sector and only 21 days per winter (31st decade in SR) for the Pacific sector.

Table 6. Decadal mean and standard deviation of the number of blocked days per winter

	Atlantic	Pacific
Observed	28.3 ± 3.2	30.7 ± 2.8
PWR	33.3 ± 4.0	22.1 ± 2.8
SR	32.9 ± 4.3	28.4 ± 3.7

Considering even longer time scales, Fig. 18 shows the longitudinal distributions of blocking frequency of 12 different periods of 50 winters extracted from the PWR integration (such periods are comparable to the length of the observed upper-air record). The maximum frequency, i.e. the frequency corresponding to the longitude of the peak in each 50-winter period, attains values ranging from 24% (Fig. 18f) to 34.5% (Fig. 18i) in the Atlantic sector. In

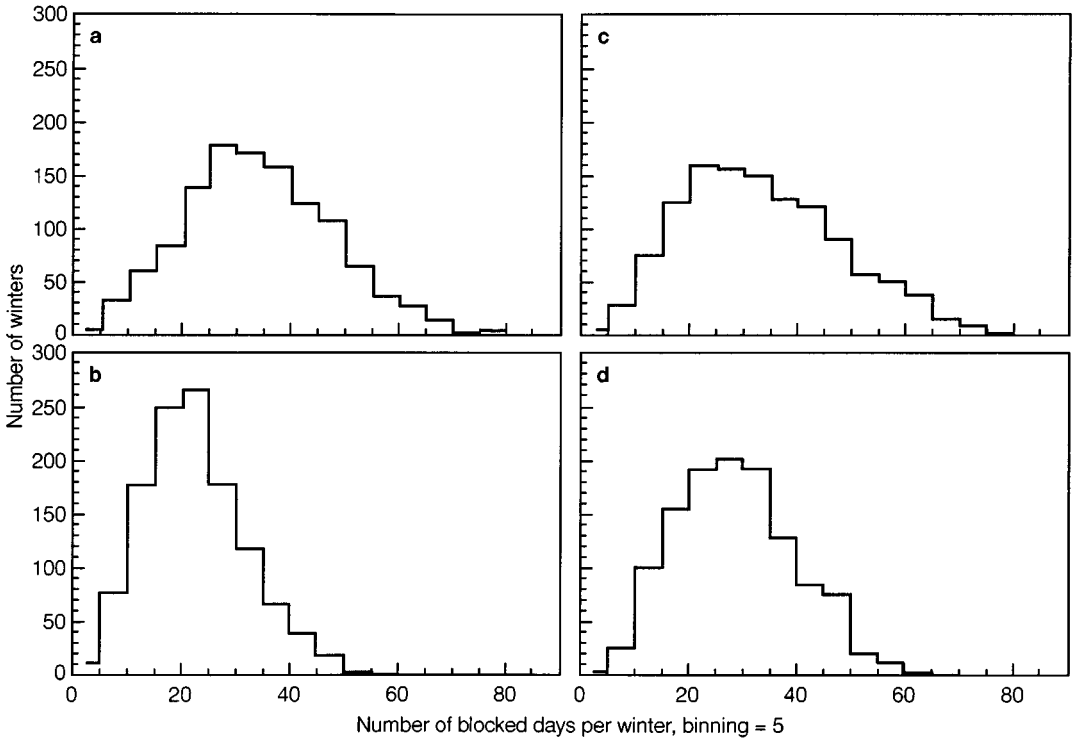

Fig. 16a–d. Distribution of winters with respect to the number of blocked days per winter: **a** Atlantic blocking in PWR. **b** Pacific blocking in PWR. **c** Atlantic blocking in SR. **d** Pacific blocking in SR

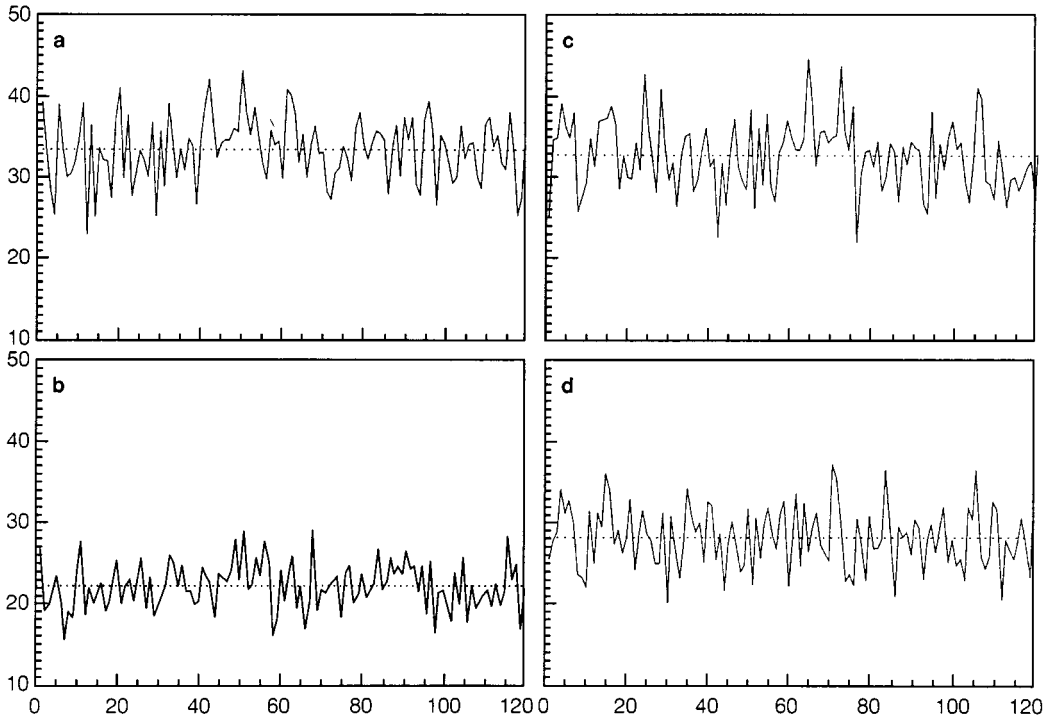

Fig. 17a–d. Time series of 10-winter means of number of blocked days per winter. **a** PWR Atlantic sector; **b** PWR Pacific sector; **c** SR Atlantic sector; **d** SR Pacific sector

the Pacific sector, the maximum frequency ranges from 13% (Fig. 18d) to 17% (Fig. 18i). As far as the number of blocked days per winter is concerned, the 50-winter averages range from 28.6 (Fig. 18f) to 37.7 (Fig. 18i) in the Atlantic sector, from 20.7 (Fig. 18d) to 24.3 (Fig. 18i) in the Pacific sector.

This variability was also identified in a power-spectrum analysis of the number of blocked days per winter, in the Atlantic and Pacific sectors, in the perpetual winter and seasonal cycle integrations. In order to have the same time interval between two consecutive winters (i.e. one year) in both integrations, a new time series was generated, extracting from the PWR one winter for every four simulated. The frequency spectra were therefore estimated using the Parzen lag-correlation method with a maximum lag of 25 years, the longest lag that was found to yield an acceptably smooth spectrum. The resulting diagrams are shown in Fig. 19. Atlantic blocking (Fig. 19a and c) exhibits higher power at all frequencies than Pacific blocking (Fig. 19b and d). At the same time seasonal cycle simulations (Fig. 19c and d) are characterised by an enhanced variability (this signal is stronger in the Pacific sector) with respect to the corresponding perpetual winter runs (Fig. 19a and b), except for Atlantic blocking variability with periods longer than 20 years. However, in both runs and sectors, the simulated fluctuations in the number of blocked days could be well represented by a white noise process.

6 Summary and discussion

The overall performance of the QG model in simulating blocking and teleconnection patterns in the Atlantic and Pacific regions is surprisingly accurate, given the simple dynamical formulation of the governing equations, where empirical forcing terms account for all physical processes not explicitly described. Both low-frequency variability phenomena are realistically simulated in the perpetual-winter run of the model as well as in the winter season of the seasonal-cycle run, the main features being stable and comparable in the two integrations.

One-point correlation maps and EOFs that correspond to the main teleconnections of the Northern-Hemisphere 500-hPa height during the winter season, i.e. the North Atlantic Oscillation and the Pacific/North American pattern, are fairly well reproduced. The NAO pattern is shifted westward, towards the North American continent, just like the Atlantic blocking sector. The PNA pattern occupies a slightly wider region, when compared to the observed pattern, extending its influence over the North Atlantic Ocean.

The fact that NAO and PNA have been found in simulations produced by a purely atmospheric model with no time-varying diabatic energy source is quite relevant to understanding their dynamics. It suggests that both teleconnections can be interpreted as preferred "internal modes" of extratropical low frequency variability. This does not, of course, discount the fact that the very same modes of oscillation may, in a number of occasions, account for the quasi-stationary response to anomalous thermal forcing from the lower boundary (SSTs) (cf. Shukla and Wallace 1983; Palmer and Mansfield 1986; Navarra and Miyakoda 1988; Ferranti et al. 1994).

Blocking in the model atmosphere occurs with higher frequency in the two oceanic regions of the Northern Hemisphere, in good agreement with observations. In the

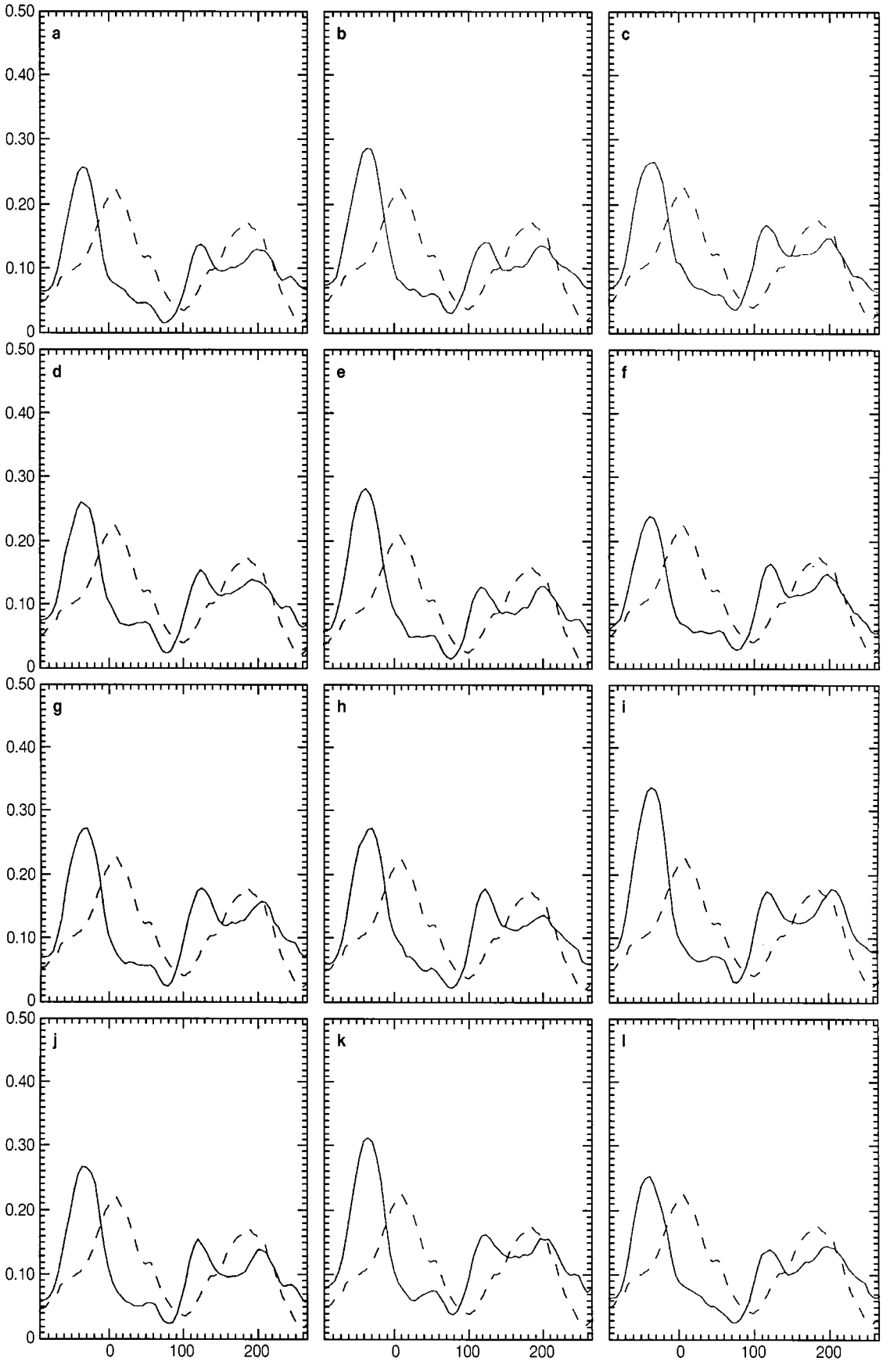

Fig. 18a–l. Blocking frequency diagrams of 12 different periods of 50 winters extracted from the PWR integration

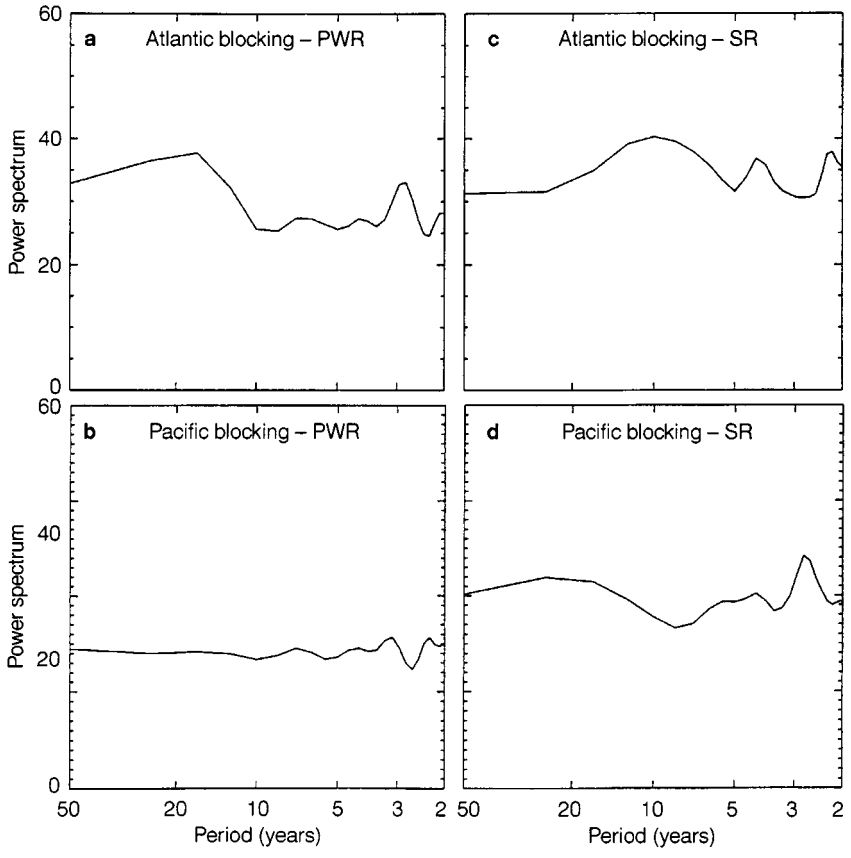

Fig. 19a–d. Power spectrum of the number of blocked days per winter: **a** Atlantic blocking in PWR. **b** Pacific blocking in PWR. **c** Atlantic blocking in SR. **d** Pacific blocking in SR

model simulations, these two regions are positioned respectively between 70 °W and 0 °E (Atlantic sector), and between 160 °E and 130 °W (Pacific sector). A tendency can be noticed to shift Euro-Atlantic blocking (cf. Rex 1950; Lejenäs and Økland 1983; Tibaldi and Molteni 1990) towards the central Atlantic Ocean, away from the western edge of the European continent. Blocking in the eastern part of the Pacific approximately covers the same region as its observed counterpart. Blocking frequency, composite maps of blocked days, and duration of blocking episodes in both sectors are all comparable with the observed climatology of the phenomenon.

The main features of blocking investigated in this work, i.e. blocking frequency and duration, are remarkably stable in the Atlantic sector, when the perpetual-winter and seasonal-cycle runs (PWR and SR respectively) are compared. In the Pacific sector, on the other hand, a significant increase in the number of blocked days per winter and in the length of episodes was observed in SR with respect to PWR, and was concentrated during the second half of the winter season. It was found that such an increase of Pacific blocking activity was primarily due to the change in the mean flow produced by the time-dependent forcing field of the seasonal integration. Therefore, it seems that Pacific blocking is more sensitive than Atlantic blocking to variations in atmospheric forcing, a result consistent with the sensitivity of Pacific blocking frequency to the representation of diabatic processes in GCM reported by Ferranti et al. (1994) and Brankovic and Molteni (1997).

In agreement with Liu and Opsteegh (1995), a considerable amount of variability of blocking activity on time scales in excess of one winter was observed in both integrations; a stronger interannual variability in blocking frequency was induced by the seasonal cycle. The QG simulations exhibit a realistic blocking variability on decadal time scales and (perhaps unexpectedly) on pluridecadal time scales. Since the external forcing is fixed, all fluctuations are ultimately the result of the internal, nonlinear dynamics of the model atmosphere. Similarly to the interdecadal variability in the zonal-mean flow investigated by James and James (1992), differences in intraseasonal variability between successive years, decades and centuries may arise just from the chaotic nature of the (modelled) atmospheric circulation. To what extent inter-decadal variability in the Earth climate system should be ascribed to purely atmospheric dynamics, rather than to coupled ocean-atmosphere modes, is still an open question.

In conclusion, the 'empirical' forcing used to keep the QG model in a realistic dynamical equilibrium seems to perform very effectively. The low-frequency statistics presented here can be favourably compared with results obtained with complex GCMs with much higher vertical and horizontal resolutions and complemented by full sets of physical parametrisations (see for example the blocking statistics analysed by Tibaldi et al. 1997). It is intriguing,

at this point, to speculate on the possible reasons for such a success.

As explained in Sect. 2.2, the empirical forcing used in the integrations can be defined as the PV tendency that would keep the observed climate as a stationary solution *minus* the mean PV tendency due to non-linear interactions of the transients. For high-frequency baroclinic transients, it is well known that their mean non-linear feedback tends to act as a sink of available potential energy and a source of kinetic energy for the time-mean flow (see Molteni 1996 for an analysis of such feedback in the context of the QG model used here). Therefore, *subtracting* the mean PV tendency from high-frequency transients means *increasing* the source of available potential energy in the forcing. It can be easily verified that omitting the high-frequency transient term in the forcing would dramatically reduce baroclinic activity in the model; therefore, the fact that such term improves the model climatology (in terms of variability) is a consequence of the importance of baroclinic energy conversion for the maintenance of the observed circulation.

In the experiments described here, however, the contribution of all transients with period shorter than 30 days, and not only of high-frequency transients, is taken into account when constructing the forcing. As mentioned already it was noted that a more realistic low-frequency variability was obtained when the contribution of low-frequency transients was included in the forcing. As in the case of baroclinic transients, this implies that energy conversions between the time-mean flow and low-frequency transients are quite important for their development. This idea can be traced back to the seminal work of Simmons et al. (1983), where the authors emphasise the importance of barotropic instability for the generation of low-frequency variability. More recently, it has been supported by the analyses of Branstator (1990, 1993) on variability in the NCAR GCM, and is also fundamental to the concept of 'neutral vectors' proposed by Marshall and Molteni (1993) as preferred axes of low-frequency variability (neutral vectors are patterns for which linear interactions with the time-mean state and dissipative tendencies are in very close balance).

The role of energy conversions from large-scale anomalies, therefore, should not be underestimated, when compared to the much more discussed and generally accepted idea that high-frequency transients provide the main source of energy for the generation of low-frequency variability. By providing objectively diagnosed mean energy sources for both high-frequency and low-frequency, the empirical forcing of the QG model produces circulation statistics which (for the winter season) are as realistic as those of some GCMs. Diagnostics of time-mean tendencies (observed and simulated by numerical models), such as those performed by Klinker and Sardeshmukh (1992) and Klinker (1994), may indeed be a valuable tool for the development of parametrisation schemes in primitive-equation models, where the contribution of different physical process to the energy sink and sources can be properly evaluated.

Acknowledgements. The work of S. Corti was supported by the Commission of the European Communities under contract EV5V-CT93-0279 (Short-term Climate variability).

References

Brankovic C, Molteni F (1997) Sensitivity of the ECMWF model northern winter climate to model formulation. Clim Dyn (in press)

Branstator G (1985a) Analysis of general circulation model sea surface temperature anomaly simulations using a linear model. Part I: forced solutions. J Atmos Sci 42:2225–2241

Branstator G (1985b) Analysis of general circulation model sea surface temperature anomaly simulations using a linear model. Part II: eigenanalysis. J Atmos Sci 42:2242–2254

Branstator G (1990) Low-frequency patterns induced by stationary waves. J Atmos Sci 47:629–648

Ferranti L, Molteni F, Palmer TN (1994) Impact of localized tropical and extratropical SST anomalies in ensembles of seasonal GCM integrations. QJR Meteorol Soc 120:1613–1645

Holton JR (1992) An introduction to dynamic meteorology. Academic Press, San Diego, pp 142–182

Horel JD, Wallace JM (1981) Planetary-scale atmospheric phenomena associated with the Southern Oscillation. Mon Weather Rev 109:813–829

Hoskins BJ, Karoly DJ (1981) The steady linear response of a spherical atmosphere to thermal and orographic forcing. J Atmos Sci 38:1179–1196

James IN, James PM (1992) Spatial structure of ultra-low frequency variability of the flow in a simple atmospheric circulation model. QJR Meteorol Soc 118:1211–1233

Klinker E (1994) Diagnosis of diabatic processes. Proc seminar held at ECMWF on Parametrization of sub-grid scale physical processes

Klinker E, Sardeshmukh P (1992) The diagnosis of mechanical dissipation in the atmosphere from large scale balance requirements. J Atmos Sci 49:608–627

Lau N-C (1981) A diagnostic study of recurrent meteorological anomalies appearing in a 15-year simulation with a GFDL general circulation model. Mon Weather Rev 109:2287–2311

Lejenäs H, Økland H (1983) Characteristic of northern hemisphere blocking as determinated from a long time series of observational data. Tellus 35A:350–362

Liu Q, Opsteegh T (1995) Interannual and decadal variations of blocking activity in a quasi-geostrophic model. Tellus 47A:941–954

Madden RA, Julian PR (1971) Detection of a 40–50 day oscillation in the zonal wind in the tropical Pacific. J Atmos Sci 28:702–708

Mak M (1991) Influences of the Earth's sphericity in the quasi-geostrophic theory. J Meteorol Soc Japan 69:497–511

Marshall J, Molteni F (1993) Towards a dynamical understanding of planetary-scale flow regimes. J Atmos Sci 50:1792–1818

Marshall JC, So WK (1990) Thermal equilibration of planetary waves. J Atmos Sci 47:963–978

Molteni F (1996) On the Dynamics of planetary flow regimes: the role of high-frequency transients. J Atmos Sci 53:1950–1971

Molteni F, Ferranti L, Palmer TN, Viterbo P (1993) A dynamical interpretation of the global response to equatorial Pacific SST anomalies. J Clim 6:777–795

Navarra A, Miyakoda K (1988) Anomaly general circulation models. J Atmos Sci 45:1509–1530

Palmer TN, Mansfield DA (1986) A study of wintertime circulation anomalies during past El Niño events, using a high resolution general circulation model. II: variability of the seasonal mean response. QJR Meteorol Soc 112:639–660

Palmer TN (1987) Modelling low-frequency variability of the atmosphere. In: Cattle M (ed) Atmospheric and oceanic variability, Royal Meteorological Society, pp 75–103

Palmer TN (1993) Extended range prediction and the Lorenz model. Bull Am Meteorol Soc 74:49–65

Rex DR (1950) Blocking action in the middle troposphere and its effect upon regional climate. II. The climatology of blocking action. Tellus 2:169–211

Roads JO (1987) Predictability in the extended range. J Atmos Sci 44 : 3495–3527

Shukla J, Wallace JM (1983) Numerical simulation of the atmospheric response to equatorial Pacific sea surface temperature anomalies. J Atmos Sci 40 : 1613–1630

Simmons AJ, Wallace JM, Branstator GW (1983) Barotropic wave propagation and instability, and atmospheric teleconnection patterns. J Atmos Sci 40 : 1363–1392

Tibaldi S, Molteni F (1990) On the operational predictability of blocking. Tellus 42A : 343–365

Tibaldi S, D'Andrea, F, Tosi E, Roeckner E (1997) Climatology of blocking in the Northern Hemisphere and in the ECHAM model. Clim Dyn 13 : 649–666.

Wallace JM, Gutzler DS (1981) Teleconnections in the geopotential height field during the Northern Hemisphere winter. Mon Weather Rev 109 : 784–812